Brazilian Journal of Geophysics (2022) 40, 2, 263–276
Brazilian Geophysical Society
ISSN 2764-8044
DOI: 10.22564/brjg.v40i2.2162

A CORRECTION FACTOR FOR THE RESISTIVITY LOG IN GAS RESERVOIRS WITH LOW RESISTIVITY PAY ZONE IN THE POTI FORMATION, PARNAÍBA BASIN, BRAZIL

Lidia Waltz Calonio [1], Caio Soares [2], Luiza Fonseca Ribeiro [1], Jeniffer Alves Nobre [1], Wagner Moreira Lupinacci [1], and Antonio Fernando Menezes Freire [1]

[1]Universidade Federal Fluminense - UFF, Niterói, RJ, Brazil
[2]ENEVA, Rio de Janeiro, RJ, Brazil

*Corresponding author email: lidiacalonio@id.uff.br

ABSTRACT. Parnaíba Basin, even being a new frontier basin, is already one of the most profitable for natural gas in Brazil. The shallow marine sandstones of the Poti Formation are the main gas reservoirs in Parque dos Gaviões. These reservoirs hold anomalously low resistivities which directly impact water saturation calculations, leading to underestimations of their true potential as gas reservoirs. We propose a method for the characterization and mitigation of the problem and for the correction of the resistivity log based on the case study of well PGN-5, seeking to obtain more adjusted results for the reservoir evaluation. The methodology used is based on the integration data, where the main inputs were drill cuttings samples, well logs, gamma-spectral data and geochemical analyzes through X-rays fluorescence. We observed that the presence of pyrite and clay minerals are the causes of the low resistivities, even in the presence of gas-charged intervals, attested by crossover between density and neutron logs and through pressure gradient data. We propose a correction factor for the resistivity log in the anomalous low resistivity zone, allowing a new evaluation of the well, leading to a significant reduction in water saturation and a remarkable net pay gain.

Keywords: low resistivity pay zone (LRPZ); petrophysics; pyrite; clay minerals.

INTRODUCTION

A common problem in petroleum reservoirs, both gas and oil, are low resistivity pay zones (LRPZ) related to the presence of clay minerals and other conductive minerals (Sneider, 2003), which affect well log evaluation, directly impacting the water saturation (SW) calculations and, therefore, the hydrocarbon volumes available in the reservoir. The conventional petrophysical interpretation is unable to identify pay intervals in low-resistivity reservoir (Chu et. al, 2011).

Several methods are currently used in order to mitigate the problem, but they are generally expensive and slow, requiring laboratory tests, special drilling fluids and specific conditions during drilling in order to work (Calonio, 2020). Often, the resistivity log in these cases can not be used, despite being an important log. This panorama is critical, especially for onshore basins, where drilling and production costs must be greatly optimized.

The exploration of hydrocarbons in Parnaíba Basin started in the 1950s, but it was only in 2010 it got the first exploratory success with the discovery of the Gavião Azul Field (Figure 1). In 2022, the Parnaíba Basin reached the mark of more than 170 wells drilled and 10 fields in Parque dos Gaviões, already occupying a prominent position among the top 20 Brazilian onshore fields with the highest production of natural gas (ANP, 2022), an exceptional result for a new frontier basin, especially considering the small area explored compared to the total area of the basin and just during a decade since the discovery of the Parque dos Gaviões. Even though Parnaíba basin is a new frontier basin with most of its area underexplored, it is already one of the most profitable for natural gas in Brazil, increasing in production and leading development and generation of infrastructure to Maranhão State, through the monetization of natural gas production in thermoelectric power plants.

The shallow marine sandstones of Poti Formation are the main reservoir in Parque dos Gaviões (Miranda et al., 2018) and present the problem of anomalously low resistivities (Menchio et al., 2020) since high resistivity values are expected for gas-filling intervals. This phenomenon impacts the water saturation (SW) calculation because the resistivity log is one of the main inputs for the evaluation. Consequently, this leads to underestimations of the gas net pay and, to overcome this problem, it is required special logs and specific evaluations by the interpreter. In order to contribute to the mitigation of this issue in gas-bearing reservoirs, we propose a workflow based on the case study of well PGN-5, drilled in Gavião Caboclo Field (Figure 1). The methodology consists in the integration of rock and log data, and the main inputs for this approach were: a) detailed description of cuttings; b) interpretation of basic set of well logs; c) gamma-spectral data measured on cuttings; and d) geochemical analysis through the X-ray fluorescence (XRF) measured on cuttings.

The first part of the workflow shows the approach to characterize the problem and the second one deals with our proposed correction for the resistivity log using cheaper and more accessible methods.

GEOLOGIC SETTING

The Parnaíba Basin is a Paleozoic intracratonic basin, located in northeastern Brazil, which occupies an area of approximately 600.000 km². It features an ellipsoidal shape oriented in the NE-SW direction with about 1.000 km on its longest axis and, in the transversal direction, it presents approximately 800 km of extension (Figure 1). At the depocenter, the total thickness reaches about 3.500 m (Vaz et al., 2007). The depositional history of the basin started after the Brazilian-Pan-African thermotectonic cycle, at the end of the Ordovician, together with other Brazilian intracratonic basins. Through borehole, seismic and gravimetric data, it was detected north-south rifts, of possibly Cambro-Ordovician age, precursors of the basin formation (Caputo et al., 2005). Also, for the same author, the marine communication with the north of Africa was blocked by an extensional collapse, related to the Eo-Hercinian orogeny. Besides, until the Eocarboniferous, the continent was invaded many times by epicontinental sea transgressions across the north of Africa.

The sedimentary succession of the basin is divided into five supersequences, which represent complete regressive-transgressive cycles (Vaz et al., 2007). The Mesodevonian-Eocarboniferous Supersequence holds the principal gas systems in this basin, where the process of thermal subsidence persisted continuously until the Eo-Hercinian orogeny that caused a discordance that marked the end of this deposition (Vetorazzi, 2012).

The Parnaíba Basin petroleum system is atypical because it is a relatively shallow basin and the maturation of the organic matter was triggered due to the elevate thermal increase provided by late magmatic intrusions (Rodrigues, 1995) of the Mosquito (Eo-Jurassic) and Sardinha (Lower Cretaceous) Formations, without which there would not have been enough thermal increment to achieve the gas generation window (Fernandes, 2011). In this sense, the main source rocks are Devonian shales of the Pimenteiras Formation (Rodrigues, 1995); on the other hand, Poti (Mississippian, Lower and Middle Carboniferous) and Cabeças (Devonian) Formations are recognized as the main reservoirs of the Parnaíba Basin in the Parque dos Gaviões area.

Regarding the quality of the Poti reservoir, there is facies variation that may reflect the coexistence of coastal environments, but the deltaic Poti sandstones have good reservoir properties in general - porosity about 18% and permeability around 240 mD (Miranda et al., 2018). According to Miranda et al. (2018), corroborated by Quiren (2020), the Poti unit can be divided into three zones: 1) the upper zone shows greater lithological homogeneity and good reservoir quality; 2) the middle interval exhibits medium quality; 3) the lower section presents the worst quality, being the most heterogeneous and laminated of all. All these facies are capable of producing gas at commercial levels. In addition, a fourth zone can be individualized close to the contact with intrusive rocks, where it is common to observe an alteration halo, of variable thickness, immediately below the sill. The contact metamorphism is harmful overall, obliterating porosity and permeability, mainly due to the recrystallization of quartz. Nevertheless, even hornfels intervals have good flow rates, enhanced by subvertical fractures occurring naturally.

The Poti Formation refers to a succession of strata that Góes and Feijó (1994) interpreted as delta deposits and tidal plains occasionally influenced by storms, reworked by waves and tides. To Góes (1995), the faciological analysis revealed that the Poti/ Longá Sequence is part of the same deltaic-estuarine-marine platform depositional sequence and can be interpreted as a coastal environment. These analyzes corroborate the interpretations of Mesner and Wooldridge (1964) who considered the lower part of the Poti Formation as marine and the upper one as fluvial-deltaic. In general, the model for deposition of Longa-Poti sedimentation corresponds to a regressive system.

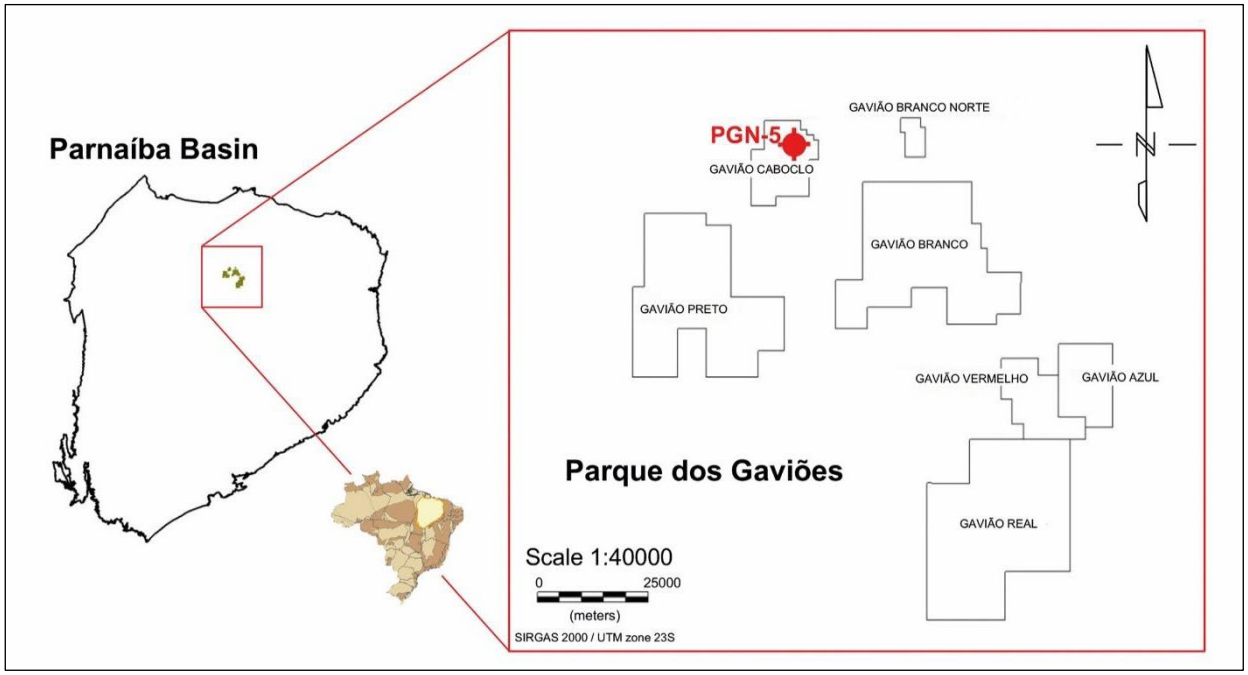

Figure 1: Location map for well PGN-5 in Gavião Caboclo Field, Parnaíba Basin.

Góes (1995) studied the Poti Formation and described the main lithotypes as constituted of sand and gravel and, subordinately, muddy rocks. Medium to fine grained sandstones predominate, while micaceous sandstones are frequent in very fine grained lithofacies. Overall, the sorting varies from moderate to good, being poorly sorted in the case of muddy sandstones. The degree of textural maturity was classed as submature to mature, in the main lithotypes, except in the muddy sandstones that are immature.

The porosity is major primary but also secondary, as a result of several generations of cementation and dissolution processes of the framework and cement grains (Góes, 1995). The author further explains that the loss of primary porosity was caused more by cementation processes than compaction ones. Góes (1995) also studied the muddy facies (shales and siltstones) with X-ray diffraction (XRD) analysis and electron microscopy. These analyses indicated a high mineralogical homogeneity and that the most common mineralogy consists of illite, kaolinite, smectite, chlorite and inter-ratified (illite, smectite and chlorite-smectite).

MATERIALS AND METHODS

In order to generate a detailed lithological profile, 64 cuttings samples of each 3-meter interval from the reservoir interval (1336/1530 m) of the PGN-5 well were initially described. These descriptions were organized in the SedLog software, from the Department of Computer Science, Royal Holloway University of London. In parallel, a preliminary evaluation was performed using the basic well log set: Caliper (CAL), Gamma Ray (GR), Density (RHOZ), Neutrons (NPOR), Resistivity (AT90), Sonic (DTCO) and Photoelectric Factor (PEFZ). The log data and the lithological interpretation were loaded in the Trace software, from K2 System, and in the Interactive Petrophysics (IP) software, from Lloyd's Register Inc.

The gas-water contact in the well was first interpreted mainly by the AT90 log and was marked at 1369 m (-1336 m), at the depth when the values for resistivity start to decrease, where it is understood that there is a change in the fluid. However, when we analyze the RHOZ and NPOR logs, the wide separation on the crossover, characteristic of gas-charged reservoirs, suggests the contact at 1418 m (-1385 m – Figure 2).

The Wireline Pressure data were obtained from the Composite Log provided by the Brazilian Petroleum National Agency (ANP). This data were plotted on the 'Pressure x Depth' graph (Figure 3) and the free water level was defined at 1418 m (-1385 m), confirming the interpretation of the RHOZ-NPOR crossover. Comparing the positioning of the two contacts, we concluded that the preliminary contact, inferred mainly by the AT90 log, was positioned incorrectly, in the interval of the reservoir still gas-charged. Therefore, with this new data, there was an increase of 49 meters of the gas column thickness.

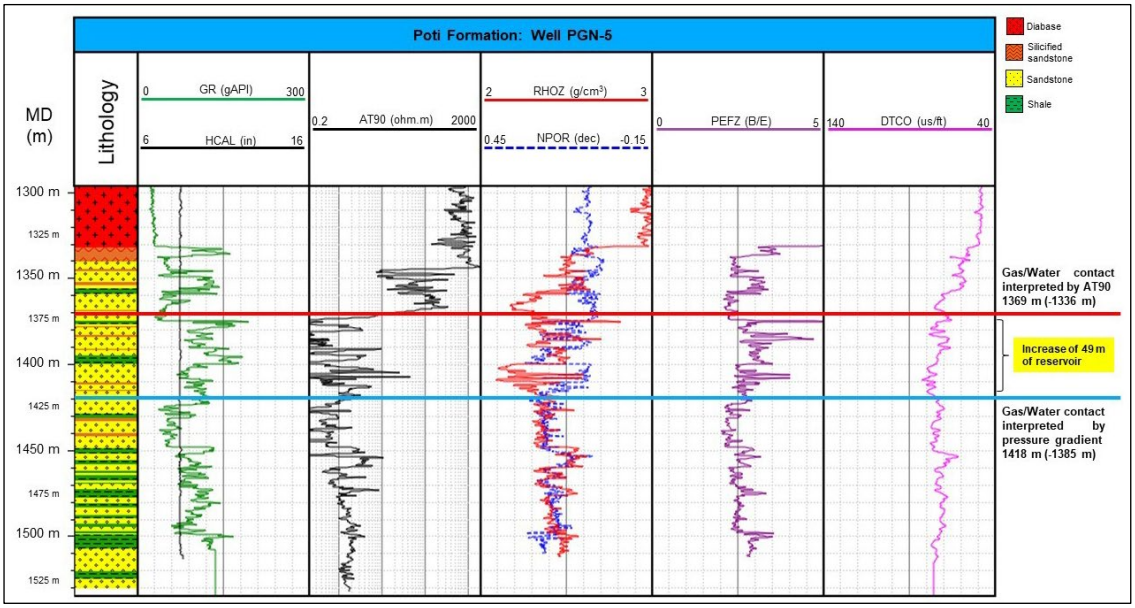

Figure 2: Logs of PGN-5 well with lithological profile reinterpreted. The difference of the free water level by the pressure gradient graph compared to the contact inferred by the resistivity log (AT90) is highlighted. From left to right: MD_Mesure Depth (m); Track 1: Reinterpreted lithology; Track 2: GR (gAPI): Gamma Ray / HCAL (in) - Caliper; Track 3: AT90 (ohm.m) - Resistivity; Track 4: RHOZ (g/cm³) - Density / NPOR (dec) - Neutron; Track 5: PEFZ (B/E) - Photoelectric factor; Track 6: DTCO (us/fe) - Sonic.

The causes of such discrepancy in well PGN-5 were studied through cuttings, logs, geochemical data from XRF analysis and gamma-spectral data, both measured on cuttings. The drill cuttings samples from the Poti Formation were available throughout the reservoir interval, except for the cored interval (1362.4 to 1379.4 m). The steps followed were:

1. Detailed description of cuttings from the interval 1336/1530 m (Poti Formation);
2. Geophysical well log loading: Gamma Ray (GR), Resistivity (AT90), Neutronic Porosity (NPOR), Density (RHOZ), Sonic (DTCO) and Photoelectric Factor (PEFZ); through these well logs a preliminary saturation evaluation was performed;
3. Rock-log integration to provide a new detailed lithological track;
4. Chemical composition identification using an energy dispersion by X-rays fluorescence (XRF) device (model Epsilon 1 by Malvern Panalytical), where two geochemical logs were generated: Iron (Fe) and Sulfur (S). Since the pyrite is an iron disulfide (FeS_2), these elements were assumed as analogs of the mineral pyrite and were also used in the elaboration of a correction factor for the anomaly observed in the resistivity log;
5. Gamma-spectral analyses to infer the type of clay minerals present, comparing the GR spectral components. The equipment used for the acquisition of these data was the portable gamma-spectrometer Radiation Solutions Inc RS-230 BGO Super-SPEC Handheld Gamma-Ray Spectrometer that provides, in each measurement, besides the radiation dose value called Total GR in nGy/h, the individualized values of potassium (K %), uranium (U ppm), and thorium (Th ppm);
6. Correction factor for the AT90 log and a new synthetic log (RT_corrected) generating using the entire data after detailing the Poti reservoir and characterizing the problem. Two evaluations were made, using the AT90 log with and without correction, and the results of water saturation and net pay were compared.

Several equations and parameters, combined in different ways and applied together with the correction factor, developed in this research, were tested to find the best petrophysical model. In the final evaluation we used the equation proposed by Larionov (1969), chosen for old rocks for Vclay; for porosity, the Gaymard and Poupon (1970) equation was used because it minimizes the gas effect; the SW was estimated by the Archie (1942) equation, which is more adequate due to the Vclay characteristics of the reservoir; and for the choice of cut-offs it was used the approach proposed by Lalanne et al. (2004).

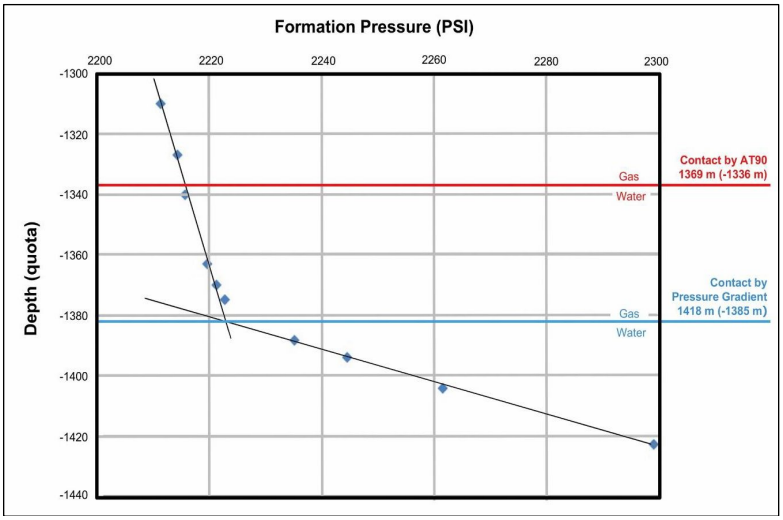

Figure 3: 'Depth x Pressure' plot used in the analysis of fluids and contacts for the well PGN-5 in the reservoir interval (Poti Formation). The free water level interpreted from the resistivity is represented by the red line and the pressure gradient data by the blue one.

RESULTS

The Parque dos Gaviões area, in Parnaíba Basin, presents the problem of anomalously low resistivities. According to Sneider (2003), the presence of minerals that increase conductivity, such as expansive argillominerals, pyrite, glauconite and others, is common in many basins worlwide. This problem demands a lithological characterization of the reservoir and, once the problem is identified, special evaluation for the correct estimation of the hydrocarbon saturation (Chu et al., 2011). The Saturation High Modeling (SHM) method has been used in these contexts, estimating saturations by logs and using laboratory data, especially the capillary pressure, not always available; the resistivity log is only used in qualitative evaluation.

In this topic we discuss the characterization of the problem in the studied well and propose a new method to deal with the resistivity curve anomaly.

Reservoir Characterization – Clay Minerals

According to Moradzadeh et al. (2011), an important task in reservoir studies is determining their characteristics to estimate their performance in terms of porosity and permeability because, without a proper and accurate characterization, many prominent errors can occur in the reservoir evaluation. Indeed, the description of cuttings revealed important characteristics of the Poti reservoir in well PGN-5. An aspect evidenced was the high clay volume of the sandstones and the intercalations with thin layers of shale, which contributes to the low resistivities as observed in the reinterpreted lithology (Figure 2).

Individualizing the type of the clay mineral from the cuttings description is not possible and some are more critical than others with regard to the cation exchange capacity (CEC), impacting therefore the AT90 log. Seeking to deal with this issue, the gamma ray spectral (GRs) data were plotted on a crossplot as proposed by Quirein (1982) and Klaia and Dudek (2016), who proposed to estimate which types of clay minerals are present based on a dispersion chart between Th (ppm) and K (%) (Figure 4).

The graph analysis suggests the presence of kaolinite and smectite. Clay is a problem for reservoirs in general, for several reasons, but here it is especially problematic because it affects the resistivity due to the presence of notably conductive clay minerals, especially the presence of smectite. According to Sneider (2003), the smectite is one of the most impacting minerals for the resistivity log because it presents a high-water content. Since the crystalline organization of the smectite has a large surface area and an excess of negative charge, which is neutralized in weak bonds by the cations present in the associated water, this clay mineral becomes effective as an adsorbent, that is, it retains many molecules by adsorption, basically water. Therefore, it is called an expansive clay mineral and its presence is especially critical, impacting the formation resistivity, decreasing it due to the large amount of interstitial and connate water that can be fixed in its internal molecular structure.

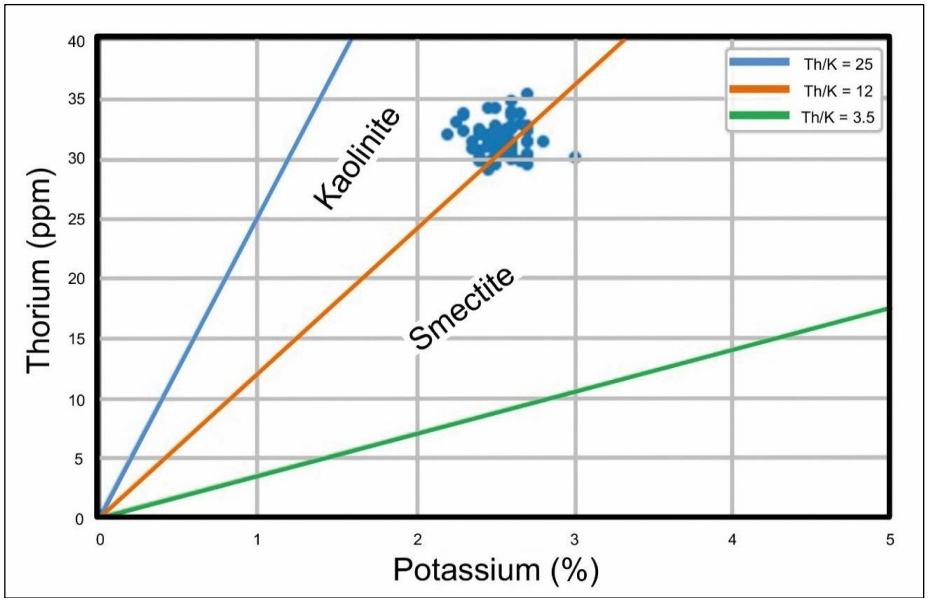

Figure 4: Scatter plot with thorium and potassium data in Poti Formation, well PGN-5, to study the type of predominant clay minerals. Modified from Klaia and Dudek (2016).

Reservoir Characterization – Pyritization

Another important characteristic that the rock data revealed during the descriptions was the abundant presence of pyrite (Figure 5). Pyrite is a conductive mineral and, if not properly corrected, leads to mistakes in water saturation in the reservoir (Clennell et al., 2010). Depositional pyrite crystals are disseminated throughout the interval analyzed, dispersed in the matrix in millimeter to submillimeter grains, euhedral faces, exhibiting its cubic crystalline habit and metallic luster. The morphology of the pyrite, as well as the size distribution and its primary textures, can be used to infer oxygenation conditions of the depositional environment (Wilkin et al., 1996). This pyrite was interpreted as having a diagenetic origin owing to its distribution, form of occurrence and morphology (Diaz, 2012).

From the XRF geochemical data, we generated curves of S and Fe and plotted them together with the other data. We used the combination of these curves as a proxy for the pyrite (FeS_2) presence and identified two geochemical facies: high sulfur and high iron zone (S-Fe_high), and low sulfur and iron zone (S-Fe_low) (Figure 6). There is a tendency to higher levels in the S-Fe_high interval, which corresponds to the area where the reservoir discloses the biggest drop down of resistivities, besides also displaying the other logs with different behavior when compared to the reservoir as a whole.

It is worth pointing out that intensely altered sandstones were observed in the interval 1330/1340 m, below the base of the diabase intrusion, often in association with these igneous fragments, indicating contact metamorphism and a potential metamorphism halo in the well, which coincides with the S-Fe_high zone (Figure 6), suggesting that the pyrite is probably related to hydrothermal fluids provided by the diabase intrusions.

Quantification of pyrite volume

Clavier (1976) and Tew (2015) bring attention to the fact that the pyrite must be in percentages higher than 5-7% and must have lateral continuity to affect the readings of the induction tool; thus, the volumetric quantification of the pyrite content was necessary in our development of the correction factor. From this, two graphs were initially applied using data from logs that aim to estimate percentages based on the work of Holmes et al. (2013) (Figure 7).

The first graph 'Density x Conductivity' (Figure 7a) is a scatter plot of the density values, extracted from the log and transformed into points, plotted against the conductivity values (C) obtained by the inversion of the AT90 log (C = 1 / AT90), also transformed into discrete points. It delimits the area where the pyrite occurs and the percentage increase of each line of the function. The second graph 'Photoelectric Factor (PE) x Conductivity' (Figure 7b) was elaborated in the same way and uses the same principle for data interpretation.

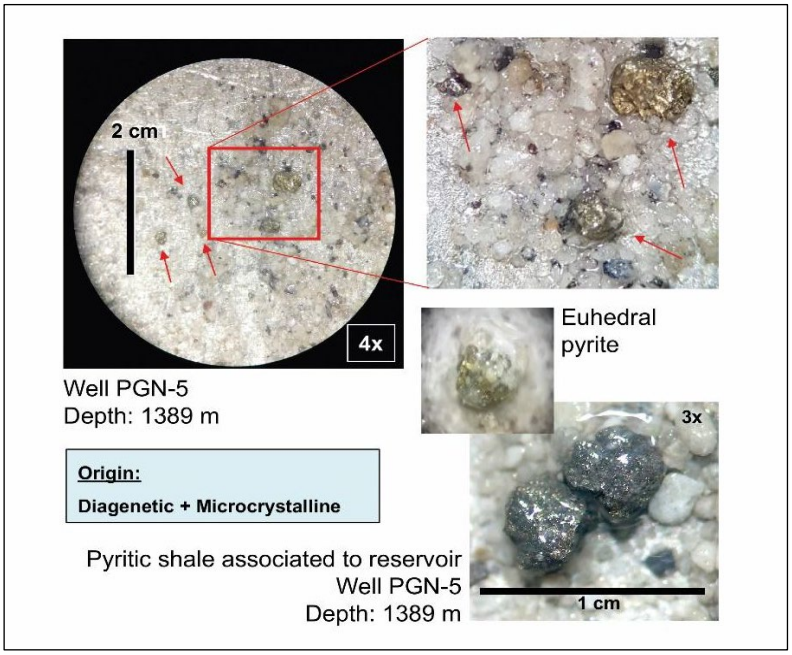

Figure 5: Pyrite crystals dispersed in the reservoir. In the shale sample there is the framboidal pyrite and in the sandstone sample euhedral pyrites.

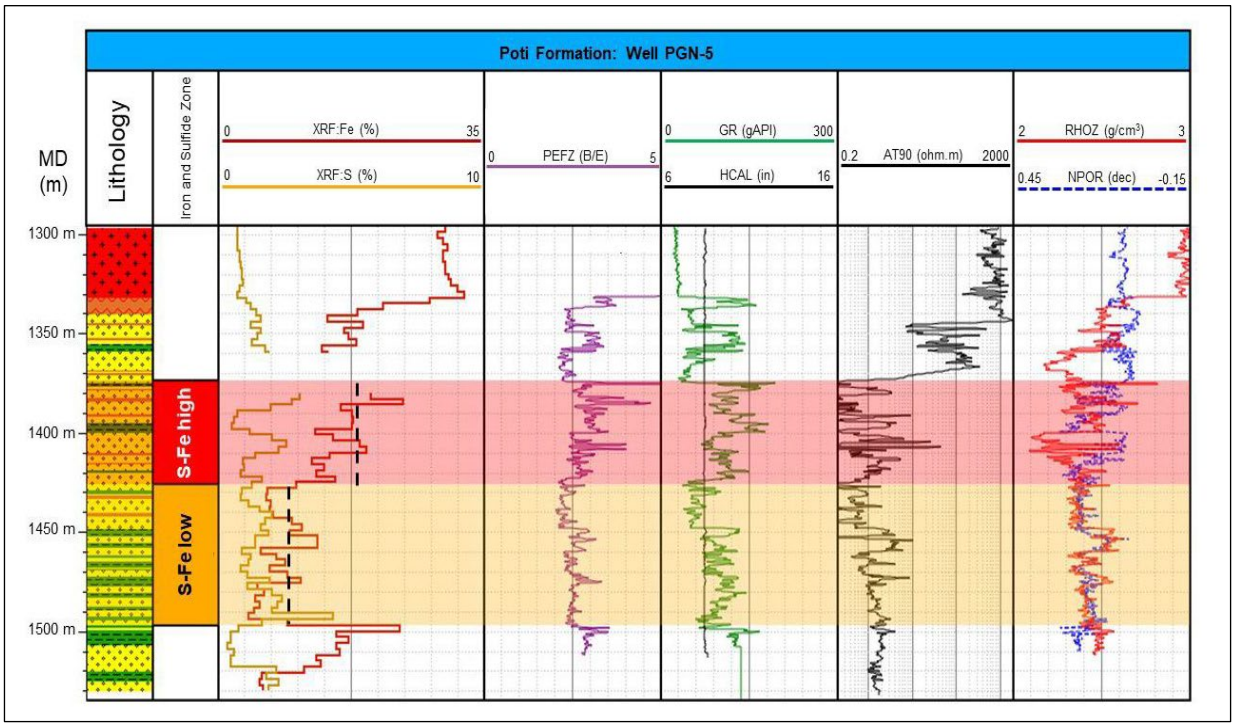

Figure 6: Reinterpreted lithological profile and logs of PGN-5 well with emphasis, in red and orange, for the two sub-areas lined off according to the values of sulfur and iron. The dashed lines in black (Track 3) show average baselines for these contents showing the increase of these elements in the zone S-Fe_high, which is in the assumed zone of influence of the igneous intrusion. From left to right: MD_Mesure Depth (m); Track 1: Reinterpreted lithology; Track 2: Individualized zones based on iron and sulfur content; Track 3: XRF - Fe (%) and XRF - S (%); Track 4: PEFZ (B/E) - Photoelectric factor; Track 5: GR (gAPI) - Gamma Ray / HCAL (in) - Caliper; Track 6: AT90 (ohm.m) - Resistivity; Track 7: RHOZ (g/cm³) - Density / NPOR (dec) - Neutron.

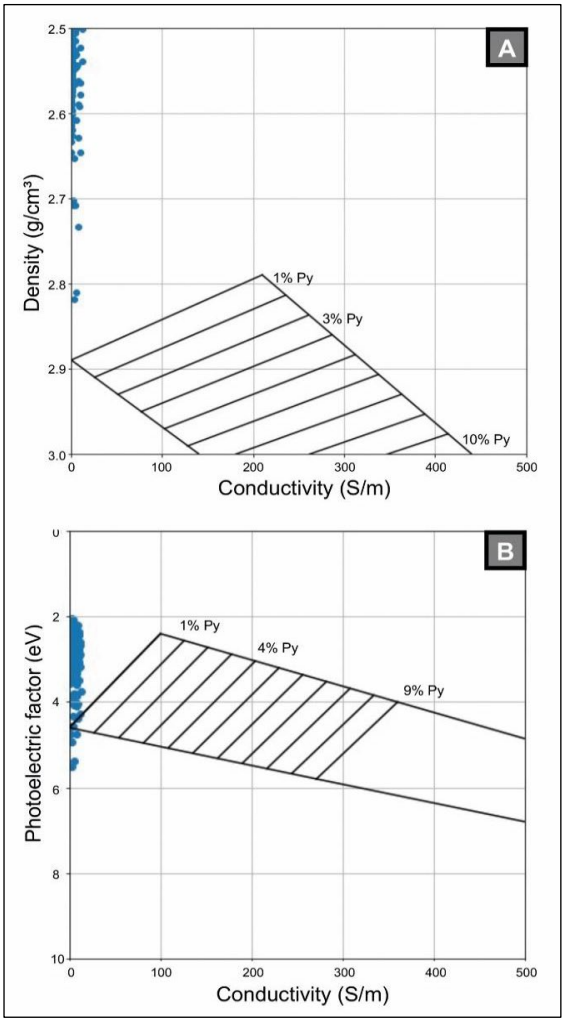

Figure 7: Charts to quantify the pyrite volume in percentage in Poti Formation, well PGN-5. (7a) "Density x Conductivity" graph; (7b) 'PE x Conductivity' graph. Modified from Holmes et al. (2013).

The results of these graphs were not as expected. Despite the large amount of pyrite observed in cuttings and in the XRF data, even frequently mentioned in the literature for the Poti reservoir, the graphs show a different scenario, indicating pyrite contents below 1% and therefore suggesting that the pyrite would not be in sufficient levels to interfere in the AT90 values, creating a paradox.

A possible reason for this ambiguity is that the pyritization occurred not only in sandstones of the reservoir in the form of euhedral pyrite crystals, but also, and mainly, in the intragranular porosity of shales in the Poti Formation, in the form of microcrystalline framboidal pyrite crystals. In fact, shale with disseminated pyrite was observed in several samples (Figure 5). So, there are two types of pyrite that occur in the reservoir and impact the tools: I) diagenetic, which can appear as framboids or euhedral crystals (Rickard et al., 1997), overall related to sandstones; and II) microcrystalline, that occurs as a substitution for organic matter in intracrystalline porosity, exhibiting a framboidal shape, present in shales and clays related to the Poti sandstone. The latter, which is difficult to identify using logs, seems to have considerable volume and lateral continuity, necessary conditions to affect the tools, as previously mentioned, being considered as the main cause for the resistivity anomaly together with the expansive clay minerals. This type of pyrite seems to impact tools in a different way, which is not detected in logs as expected, and requires further studies to understand its effects on the logs considering, above all, the lateral resolution of the tools, because AT90 is able to read deeper than the photoelectric factor and density, besides the different vertical resolution between the logs, which may read a greater or lesser mixture of the lithologies, attenuating the effect of the pyrite on the logs, and impacting therefore the use of these graphs and the interpretation.

Another important point to consider is that the gas fluid itself interferes with the logs, impacting the readings and potentially affecting the application of these graphs; moreover, these logs are impacted not only by pyrite but also by expansive clays.

The Development of a Correction Factor

The AT90 log is drastically affected by pyrite and clay minerals in the interval 1375/1430 m, besides the "gas effect" observed in the crossover RHOZ/NPOR (Figure 2) and proved by the pressure gradient of gas (Figure 3), indicating high gas saturation despite the low resistivity. In this interval, the SW calculation is severely affected and about 49 m of gas net pay is underestimated. In this way, using geochemical data, we propose a correction factor to mitigate the impact of the conductivity given by pyrite and clay minerals.

This factor allows the pseudo correction of the AT90 log using a combination of the induction log and the Fe and S curves, where the conductivity effect of the pyrite is unconsidered and the saturation calculation can be redone from the pseudo corrected resistivity log. The correction for the AT90 was used in the affected interval and this new log provided an estimation for the reservoir more consistent with the gas saturation suggested by RHOZ-NPOR crossover and wireline pressure data.

We assumed that the original AT90 log displays low values due to an increase in conductivity, given by the presence of pyrite and clay minerals, so removing

this effect is what needs to be done. Initially, two zones were individualized within the gas reservoir interval, Rtx and Rty (Figure 8). On one hand, the upper Rtx zone (Figure 8) corresponds to AT90 taken as a basis for values assumed to be "regular" considering a gas interval, that is, less affected by pyrite, with lower levels of S and Fe. On the other hand, the Rty zone (Figure 8) corresponds to an AT90 log considered anomalously low, commonly referred to in the literature as low resistivity pay zones (LRPZ), besides also related to a gas-charged interval. Therefore, the Rty interval demands correction for a better SW calculation, being here the point where the reservoir is underestimated when the input in the saturation calculation is the original AT90 log. It is in this zone, where S-Fe has high values, that the correction factor was applied.

Since the pyrite content and resistivity are inversely proportional, a relationship between them was described (Equation 1):

$$\begin{aligned} &\text{S-Fe\_normal X} \rightarrow \text{Rt\_normal} \\ &\text{S-Fe\_high Y} \rightarrow \text{Fw*Rt\_affected} \end{aligned} \quad (1)$$

Where:

1. S-Fe_normal X: Fe and S contents read at a point with 'standard' resistivity;
2. Rt_normal: Resistivity read at a point where it is not affected and has 'regular' values;
3. S-Fe_high Y: Fe and S contents read at a point with affected resistivity;
4. Rt_affected: Resistivity read at the point where the LRPZ is;
5. Fw (conductivity factor): An empirical mediator between the variables, applied in a way to remove the conductivity given by pyrite and to 'fix' the inverse relationship between the terms of the equation.

Values (1) and (2) were extracted from the point 1435 m (Figure 2), chosen for presenting the expected resistivity for water saturation = 100% in a sandstone below the gas interval. Its characteristics are: a) 'clean' sandstone (GR = 59 gAPI) inside the reservoir; b) water zone with ordinary resistivity (Rtwa <0.2 ohm.m); c) low values of S-Fe (Fe = 7%; S = 1.1%); values (3) are Fe and S read for intervals of 3 meters (cuttings interval); values (4) are from each point of the affected AT90 log (LRPZ); and for the values of the cored interval, where there are no cuttings, an average was applied; Fw (Equation 2) is calculated from the replacement of the above values in the development of the rule of three. Thus, we have:

$$\text{Fw} = (\text{S/Fe\_high}) / (\text{Rt\_affected}) \times (\text{Rt\_normal}) / (\text{S/Fe\_normal}) \quad (2)$$

Replacing the values for well PGN-5 (Equation 3):

$$\text{Fw} = 1.27 \times [(\text{S/Fe\_high}) / (\text{Rt\_affected})] \quad (3)$$

A second component that integrated the correction factor tests and showed consistent results was the sum of the value 116.55 obtained by subtracting the averages of Rtx and Rty (Equation 4):

$$\begin{aligned} \text{Rtx\_ average} &= 119.30 \text{ ohm.m} \\ \text{Rty\_ average} &= 2.753 \text{ ohm.m} \\ \text{Rtx\_average - Rty\_average} &= 116.55 \text{ ohm.m} \end{aligned} \quad (4)$$

Since the values of the Rtx zone are considered to be affected by pyrite, it was possible to infer the expected resistivity for the affected Rty zone. In this way, a subtraction of the average resistivities of the Rtx and Rty zones was made and considered in the correction calculations.

Several tests were performed in the Rty zone, applying the Fw factor and the average Rtx-Rty in different combinations of equations. The results were loaded in the IP and compared to the unaffected zone as a parameter; therefore, the best one was empirically chosen (Equation 5) to the final evaluation where the formula was applied point to point on the AT90 log, generating the corrected resistivity log (RT_corrected) (Figure 8).

$$\text{RT\_corrected} = \text{Rty\_affected} + (116.55*\text{Fw}) \quad (5)$$

As shown in Figure 8, the reservoir was re-evaluated based on the RT_corrected and presented good results when compared to the calculations of the original AT90. Using the original resistivity (black log on track 8) we see a very high water saturation (Rty zone on track 12). The net pay (in red on track 17) is very low. On the other hand, the evaluation applying the corrected resistivity (blue log on track 8) shows significant reduction in water saturation (Rty zone on track 13), generating a remarkable net pay gain (in green on track 17) in the corrected zone. As seen previously, this result is supported and showed to be consistent with the crossover of the RHOZ and NPOR (track 6) logs and the pressure gradient graph (Figure 3), through which the gas carrier interval was identified.

For saturation calculations, several equations were tested. Simandoux (1973) and Archie (1942) showed the best results, but from calibration with laboratory data, Archie (1942) was used in the final evaluation. Although Simandoux (1933) is more

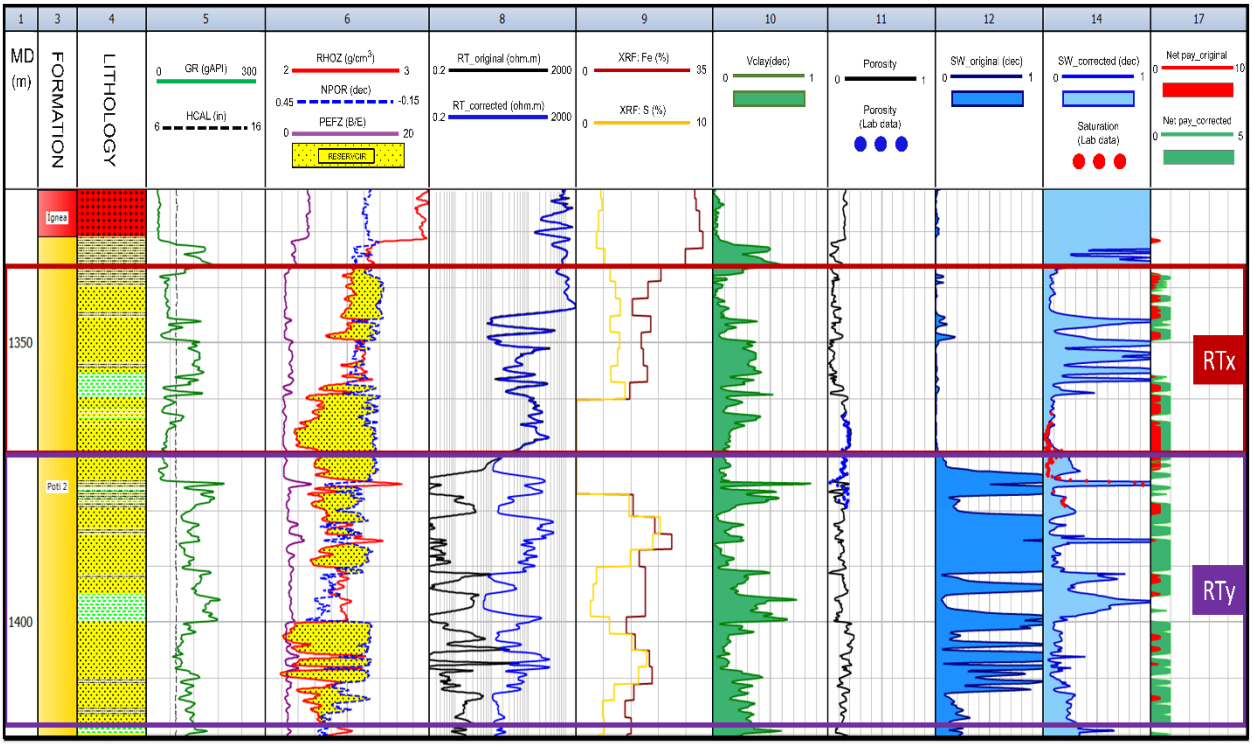

Figure 8: Well logs of PGN-5. From left to right: Track 1 - MD_Mesure Depth (m); Track 3: Formation; Track 4: Reinterpreted lithology; Track 5: GR (gAPI) - Gamma Ray / HCAL (in) - Caliper; Track 6: RHOZ (g/cm³) - Density / NPOR (dec) - Neutron / PEFZ (B/E) - Photoelectric factor; Track 8: RT_original (black) - Original resistivity (ohm.m) / RT_corrected (blue) - Corrected resistivity (ohm.m); Track 9: XRF - Fe (%) and XRF - S (%); Track 10: Vclay (%) - Clay volume calculated by Larionov (1969) equation; Track 11: Porosity (%) calculated by Gaymard and Poupon (1970) equation / Porosity (%) obtained from lab data; Track 12: SW_original (%) - water saturation calculated from resistivity log without correction using Archie (1942) equation; Track 14: SW_corrected (%) - water saturation calculated from resistivity log with correction using Archie (1942) equation / Saturation (%) obtained from lab data; Track 17: Net pay_original (red) and Net pay_corrected (green). The Rtx (normal) and Rty (corrected) zones are highlighted.

suitable for rich clay reservoirs since it considers other conductive materials besides water, Archie (1942) proved to be more adequate because it is better to describe the reservoir zones characterized as clean sandstone.

DISCUSSION

The results pointed out that pyrite and clay minerals are the causes of the low resistivities observed in well PGN-5. The presence of microcrystalline pyrite, present in the microporosity of the shales, often interbedded with the sandstones, proved to be critical for the observed anomaly. The interpretation of the data suggests that the origin of the pyrite seems to be associated with the magmatism present in the Formation Poti. The LRPZ requires special evaluations and the developed correction factor showed robust and coherent results, enabling it to be replicated in other wells with similar XRF and log features, where pyrite and clay minerals are the origin of the problem in siliciclastic environments and also in the presence of gas fluid.

A brief comparison with the more usual SHM method to deal with the issue is discussed below, including the quality control of the proposed methodology as well as the origin of the reservoir pyritization.

Quality Control of the Proposed Method

A comparison with laboratory data was conducted for quality control of the proposed methodology. In Figure 8 (track 14) we observe the saturation calculated from RT_corrected and the saturation data measured in the lab, where we see that the results present a correlation of 0.82 (82%). In this sense, a crossplot (Figure 9) was made between these data, indicating consistency for the use of RT_corrected in the final saturation evaluations.

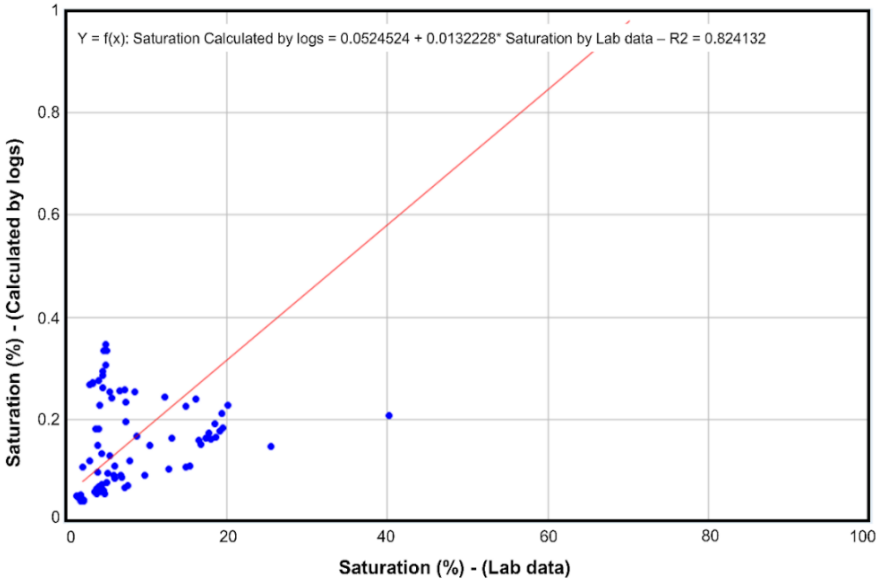

Figure 9: Crossplot of the laboratory saturation data versus the saturation calculated with the corrected resistivity curve.

Some considerations can be made concerning the final evaluation of water saturation with the corrected resistivity, especially in the interval where the laboratory data indicate a saturation lower than the one calculated by the logs, in the very beginning of Rty. This may be due to the correction of the curve itself, which in this interval was done with average values, since it is the interval where the cuttings samples were not obtained. The calculations also considered the porosity, which in this interval decreases significantly due to a drop in the density log, apparently reflecting lithological characteristics that the logs cannot detect, being the laboratory data much more accurate.

We can also mention that the Archie (1942) equation sometimes indicates high water saturation between gas intervals. More studies are needed to evaluate if these are permeability barriers or if it is more appropriate to use different methods for different clay zones within the reservoir.

In the study area, another method that was applied to get better estimates of hydrocarbon saturation is the Saturation High Modeling (SHM); however, the use of data integration and resistivity log correction, proposed in this research, has some advantages over the SHM application. First, we can cite that the resistivity log is discarded for quantitative evaluations, despite their importance, and, in the proposal of the present research, it can be used. We can also mention that the SHM methodology is based on the analysis of capillary pressure data to predict the distribution of fluids and the initial water saturation of a reservoir, which is more effective if calibrated using core data (Valentini et al., 2017), that are relatively uncommon and expensive. In addition, the problem of LRPZ in the world, has been solved with methodologies that involve the use of nuclear magnetic resonance (NMR) and special well logs, particularly expensive for onshore contexts. Chu et al. (2011), for example, explain in their work that the calibration is based on a good relationship recognized among water saturations from capillary pressure data in comparison to that estimated from NMR core. Hamada et al. (2002) also present an approach using NMR. In the present work we propose to use cheaper and available data, such as the cuttings samples and logs, and to use XRF for the chemical analyses, which is cheaper as well.

On the other hand, Pillai et al. (2015) bring a case study where the integration of the advanced and standard logging tool is used to reveal the true potential of a gas reservoir in an Australian field, but it is worth mentioning that, for the use of special logs, we must be aware of the problem before drilling, which does not occur in the first well, as it can lead to decisions to abandon the prospect. The correction factor can be applied after drilling and without the use of special logs.

We can also mention Pratama et. al (2017) and Audinno et. al (2016) who work with a combination of scanning electron microscope (SEM) and XRD analysis for the petrographic analysis in cores and side well coring sampling. In general, SEM and cores are not accessible data due to the cost. In addition, Klimentos et al. (1195) proposed a quantification of the volume of pyrite, calculated from logs in conjunction with SEM, XRD, thin-section and core-analysis studies. The

methodology proposed in this research applies a more affordable approach when using XRF for the quantification of pyrite and clay minerals, allowing an analysis of the reservoir even in the absence of mineralogical analysis by XRD. This approach can be extrapolated to several applications in the mineralogical characterization of reservoirs.

The Origin of Pyrite

The crystallization of pyrite demands availability of sulfur and iron and anoxic environmental conditions (Rickard et al., 1997). As seen before, we observed the presence of euhedral and framboidal pyrite in the reservoir impacting the logs. The microcrystalline pyrite, in particular, seems to be the major cause of the anomalously low resistivity together with the reservoir clayness characterized as composed of expansive clays. The two generations of pyrite crystals suggest that the framboid grains are syndepositional, nucleated with organic material, and that the euhedral crystals are diagenetic and/or hydrothermal, associated with fluids from intrusions (Sageman et al., 2003). Indeed, Góes (1995) and Miranda et al. (2014) approach, in their work studies, the mineralogy of Parnaíba Basin through scanning electron microscopy and X-ray diffraction and describe the presence of microcrystalline (framboidal) pyrite nucleated in organic material, dispersed in the matrix and occurring in substitution to the organic matter filling the intracrystalline porosity shales.

In the studied well, the depositional context favors the pyritization of the Poti reservoir, as seen in the topic Geologic Setting, and, according to Miranda (2014), the high concentration of organic matter suggests reducing conditions for deposition in a complex coastal environment, enabling us to interpret that the availability of sulfur would come from organic matter, deposited and preserved in anoxic conditions, due to successive drowning episodes, quickly overlapped by sandy deltaic sedimentation (Miranda, 2014).

The source of iron, on the other hand, would come from basic magmatism, from the magmatic events Mosquito (Early Jurassic) and Sardinha (Lower Cretaceous), affecting all adjacent lithologies, source rocks and reservoirs, with the percolation of fluids induced by the intrusions themselves. The sulfur can also originate from these magmatic events.

Then, these high levels of iron (Figure 6) seem intrinsically associated with the percolation of hydrothermal fluids associated with diabase intrusions present in Poti Formation. In turn, the sulfur is related with organic matter, whose preservation is related to a reducing environment, suitable for the precipitation of sulfides (Morse, 1994). Since the intruded igneous rocks favor the percolation of fluids enriched in iron, when grouped with the sulfur present in the organic matter, preserved in anoxic environment, they support the crystallization of pyrite.

Regarding the clay content of the reservoir, in parallel with the gamma-spectral analyses, description of the cuttings and reinterpretation of the lithological profile, Góes (1995) also studied the muddy facies through XRD and electron microscopy, disclosing that the most common clay minerals are illite, kaolinite, smectite, chlorite and inter-ratified (illite, smectite and chlorite-smectite), supporting the interpretations in this work.

CONCLUSIONS

The Poti reservoir in well PGN-5 presents the LRPZ. The gas-water contact was reinterpreted, resulting in an increase of 49 meters of the gas column. The study revealed a clay and pyrite bearing, which causes the anomaly in resistivity. Pyrite was interpreted as having a diagenetic and microcrystalline origin, replacing organic matter in the microporosity of clays and shales, both potentially related to the percolation of fluids induced by the Jurassic-Cretaceous magmatism of the basin, but the latter being more critical to the changes seen in the AT90 log induction measurements. Clay minerals were characterized as predominantly composed by kaolinite and smectite, which show high cation exchange capacity (CEC), inferred from gamma-spectral data. Therefore, the framboidal pyrite and expansive clay minerals were interpreted as the main causes of the LRPZ occurrence. The interval with the highest iron and sulfur content presents the most severe problem in the behavior of the AT90 log and, with the data of S and Fe, a correction factor was proposed. This correction factor allowed the elaboration of a corrected resistivity log that was used for a new evaluation of the reservoir, generating a significant reduction in water saturation and a remarkable net pay gain in the corrected zone. The laboratory data indicated that the methodology is consistent for the correction of the resistivity log. This workflow can be applied to reservoirs with similar characteristics, with the integration of rock-log data being essential for the results and conclusions reached. The workflow presents two parts, that can be applied apart: the first is the characterization and the second is the correction. To improve the correction factor and understand the impact of microcrystalline pyrite on the logs, this workflow should be extended to more wells.

REFERENCES

Audinno, R. T., I. P. Pratama, A. Halim, and D. P. Kusuma, 2016, Integrated Analysis of The-Low Resistivity Hydrocarbon Reservoir in the "S" Field: IPA 40th Annual Convention and Exhibition, Jakarta, 1–12.

Calonio, L. W., 2020, Influência de pirita e argilominerais nos cálculos de saturação da Fm. Poti, Bacia do Parnaíba: um estudo de caso no poço 3-PGN-5-MA: M.S. thesis, Universidade Federal Fluminense, RJ, Brazil. 160 pp.

Caputo, M. V., R. Iannuzzi, and V. M. M. Fonseca, 2005, Bacias sedimentares brasileiras: Bacia do Parnaíba: Phoenix, **81**, 1–6.

Chu, W.-C., and J. Steckhan, 2011, A practical approach to determine low-resistivity pay in clastic reservoirs: SPE Annual Technical Conference and Exhibition, Denver, CO. DOI: 10.2118/147360-MS.

Clavier, C., A. Heim, and C. Scala, 1976, Effect of pyrite on resistivity and other logging measurements: SPWLA 17th Annual Logging Symposium, Ridgefield, CT, 1–34.

Clennell, M. B., M. Josh, L. Esteban, C. D. Piane, S. Schmid, M. Verrall, D. Hill, C. Woods, and B. McMullan, 2010, The influence of pyrite on rock electrical properties: A case study from NW Australian gas reservoirs: SPWLA 51st Annual Logging Symposium, Perth, Western Australia. DOI: 10.13140/2.1.4026.0483.

Díaz, R. A. R., 2012, Geoquímica do enxofre e morfologia da pirita em sedimentos do sistema de ressurgência de Cabo Frio (RJ): M.S. thesis, Universidade Federal Fluminense, RJ, Brazil. 113 pp.

Fernandes, R. F., 2011, Estudo da evolução termomecânica da Bacia do Parnaíba: Ph.D. dissertation, Universidade Federal do Rio de Janeiro, RJ, Brazil. 116 pp.

Góes, A. M., 1995, Formação Poti (Carbonífero inferior) da Bacia do Parnaíba: Ph.D. dissertation, Universidade de São Paulo, SP, Brazil. 204 pp.

Góes, A. M. O., and F. J. Feijó, 1994, Bacia do Parnaíba: Boletim de Geociências da Petrobras, **1**, 57–68.

Hamada, G. M., and M. N. Al-Awad, 2002, Evaluation of low resistivity beds using nuclear magnetic resonance log. Eng. Sci. Technol., 99–105. DOI: 10.4197/Eng.14-1.3.

Holmes, M., A. Holmes, and D. Holmes, 2013, A Petrophysical Model to Quantify Pyrite Volumes and to Adjust Resistivity Response to Account for Pyrite Conductivity: 2013 AAPG ACE, Pittsburgh, PA, 19–22.

Klaja, J., and L. Dudek, 2016, Geological interpretation of spectral gamma ray (SGR) logging in selected boreholes: Nafta-Gaz, **72**, 1, 3–14. DOI: 10.18668/NG2016.01.01.

Klimentos, T., 1995, Pyrite volume estimation by well log analysis and petrophysical studies: SPWLA, **36**, 6, SPWLA-1995-v36n6a1.

Lalanne, B. J., and G. J. Massonnat, 2004, Impacts of petrophysical cut-offs in reservoir models: SPE Annual Technical Conference and Exhibition, Houston, TX, 26–29. SPE-91040-MS. DOI: 10.2118/91040-MS.

Campos, C. W. M., 1964, Estratigrafia das bacias paleozoica e cretácea do Maranhão: Bol. Técnico da Petrobras, **7**, 2, 137–164.

Menchio, B., and M. Yebra, 2020, The importance of core-log integration in laminated reservoirs with complex mineralogy: case study of Longá Formation, a new exploratory play in the Parnaíba Basin, Brazil: SPWLA 61st Annual Logging Symposium, June 24–July 29, Virtual Online Webinar. DOI: 10.30632/SPWLA-5007.

Miranda, F. S., 2014, Caracterização geológica da Formação Pimenteiras como potencial reservatório do tipo shale-gas (Devoniano da Bacia do Parnaíba): Ph.D. dissertation, Universidade Federal do Rio de Janeiro, Brazil. 257 pp.

Miranda, F. S., A. L. Vettorazzi, P. R. Da Cruz Cunha, F. B. Aragão, D. Michelon, J. L. Caldeira, E. Porsche, C. Martins, R. B. Ribeiro, A. F. Vilela, J. R. Corrêa, L. S. Silveira, and K. Andreola, 2018, Atypical igneous-sedimentary petroleum systems of the Parnaíba Basin, Brazil: seismic, well logs and cores: Geol. Soc. Lond., Special Publications, **472**, 1, 341–360. DOI: 10.1144/SP472.15.

Moradzadeh, A., and M. R. Bakhtiari, 2011, Methods of water saturation estimation: Historical perspective: JPGE, **3**, 2, 45–53.

Morse, J. W., 1994, Interactions of trace metals with authigenic sulfide minerals: implications for their bioavailability: Marine Chemistry, **46**, 1–2, 1–6. DOI: 10.1016/0304-4203(94)90040-X.

Pereira, R. M., 2020, Interpretação paleodeposicional da Formação Cabeças a partir de dados gamaespectrais de poços da área do Parque dos Gaviões, Bacia do Parnaíba: M.S. thesis, Universidade Federal Fluminense, RJ, Brazil. 122 pp.

Pillai, P., Boyle, K., Toumelin, E., and Kho, D., 2015, Advanced Formation Logging: A case study of revealing the true potential of a gas Reservoir: SPWLA 56th Annual Logging Symposium, Long Beach, CA, 18–22.

Pratama, E., M. Suhaili Ismail, and S. Ridha, 2017, An integrated workflow to characterize and evaluate low resistivity pay and its phenomenon in a sandstone reservoir: JGE, **14**, 3, 513–519. DOI: 10.1088/1742-2140/aa5efb.

Quirein, J. A., J. S. Gardner, and J. T. Watson, 1982, Combined Natural Gamma Ray Spectral/Litho-

Density Measurements Applied to Clay Mineral Identification: AAPG Bulletin, **66**, 9, 1446–1446.

Rickard, D., 1997, Kinetics of pyrite formation by the H_2S oxidation of iron (II) monosulfide in aqueous solutions between 25 and 125°C: The rate equation: GCA, **61**, 1, 115–134. DOI: 10.1016/S0016-7037(96)00321-3.

Rodrigues, R., 1995, A geoquímica orgânica na Bacia do Parnaíba: Ph.D. dissertation, Universidade Federal do Rio Grande do Sul, RS, Brazil. 252 pp.

Sageman, B. B., A. E. Murphy, J. P. Werne, C. A. Ver Straeten, D. J. Hollander, and T. W. Lyons, 2003, A tale of shales: the relative roles of production, decomposition, and dilution in the accumulation of organic-rich strata, Middle–Upper Devonian, Appalachian basin: Chem. Geol., **195**, 1-4, 229–273. DOI: 10.1016/S0009-2541(02)00397-2.

Sneider, R. M. 2003, Worldwide examples of low resistivity pay, *in*: Sternbach, C. A., M. W. Downey, and G. M. Friedman, eds., Discoverers of the 20th Century: Perfecting the Search AAPG Special Publication, Houston, 47–59.

Tew, A. T., 2015, Impact of Conductive Minerals on Measurements of Electrical Resistivity: Ph.D. dissertation, Stanford University, 151 pp.

Valentini, S., D. Bernorio, M. Grandis, A. Mazzacca, A. Serrao, and L. Visconti, 2017, Saturation height modelling: an integrated methodology to define a consistent saturation profile: Offshore Mediterranean Conference and Exhibition, Ravenna, Italy, 29–31.

Vaz, P. T., N. G. A. M. Rezende, J. R. Wanderley Filho, and W. S. Travassos, 2007, Bacia do Parnaíba: Boletim de Geociências da Petrobras, **15**, 2, 253–263.

Vettorazzi, A. L. S., 2012, Caracterização sedimentológica dos arenitos da Formação Cabeças (Devoniano) na borda leste da Bacia do Parnaíba: M.S. thesis, Universidade Federal do Rio de Janeiro, RJ, Brazil. 103 pp.

Wilkin, R. T., H. L. Barnes, and S. L. Brantley, 1996, The size distribution of framboidal pyrite in modern sediments: an indicator of redox conditions: GCA, **60**, 20, 3897–3912. DOI: 10.1016/0016-7037(96)00209-8.

CALONIO, L. W.: correction factor development, well evaluation, drill cuttings sample description, lithology reinterpretation, geochemical and gamma-spectrometry analysis interpretation, all data integration, literature review, paper writing; **SOARES, C**.: Support for well log evaluation in the software IP; **RIBEIRO, L. F**.: XRF data generating from the drill cuttings samples; **NOBRE, J. A**.: gamma-spectometry generating from the drill cuttings samples; **LUPINACCI, W. M**.: co-supervisor of the correction factor development**; FREIRE, A. F. M.:** research project development guidance.

Received on December 28, 2021 / Accepted on July 28, 2022

CC BY - Creative Commons attribution-type BY